Temperature-Induced Topological Phase Transitions: Promoted versus Suppressed Nontrivial Topology

Gabriel Antonius and Steven G. Louie

Phys. Rev. Lett. **117**, 246401 — Published 7 December 2016

DOI: 10.1103/PhysRevLett.117.246401

Temperature-induced topological phase transitions: promoted vs. suppressed non-trivial topology

Gabriel Antonius* and Steven G. Louie
Department of Physics, University of California at Berkeley, California 94720, USA and Materials Sciences Division, Lawrence Berkeley National Laboratory, Berkeley, California 94720, USA

Contrary to previous two-band model studies which find increasing temperature would induce a topological phase transition, we show here through first-principles calculations that the opposite is also realizable, depending on the material's full band structure and symmetry of the electron-phonon coupling potential. This finding explains recent experimental results by Wojek *et al.* [Nature Communications 6, 8463 (2015)]. We show that the topological phase diagram of $BiTl(S_{1-\delta}Se_\delta)_2$ as a function of doping and temperature contains two distinct regions with non-trivial topology. In $BiTlS_2$, the phonons promote the topological phase at high temperature, while in $BiTlSe_2$, the system is driven back into the trivial phase.

PACS numbers: 63.20.kd, 63.20.dk, 65.40.-b, 71.15.Mb

Recent studies on three-dimensional topological insulators have identified several materials with tunable topological phases [1]. Upon varying experimental parameters, these materials undergo a phase transition between a trivial and a topological insulator state. Such transition may occur as a function of impurity doping [2–5], pressure [6–8], or temperature [4, 9–12]. The effect of temperature becomes especially important for devices that are expected to operate under varying conditions [13]. It is thus desirable to be able to predict the topological phase diagrams of these materials and their physical origin.

Electron–phonon interactions underly the temperature-induced topological phase transition. As more phonons are being thermally activated, the electronic band energies may shift and close the band gap until a band inversion occurs at some critical temperature. This process was first described in 2D and 3D topological insulators from model hamiltonians [14–18]. First-principles calcualtions later confirmed that lattice deformation due to phonons could flip the Z_2 invariant [19][20].

One remarkable prediction from Garate *et al.* [14, 15] was that electron–phonon coupling could induce a trivial to topological phase transition with increasing temperature. The requirement for this scenario to happen is a negative temperature coefficients for the band edge states in the trivial phase, which promotes a band inversion at high temperature and stabilizes the topological phase. They proposed that such phenomenon could be seen in $BiTl(S_{1-\delta}Se_\delta)_2$, due to the presence of light atoms and the tunability of the band gap with doping. While no temperature-dependent measurements have been reported in this particular material, those performed in $Pb_{1-\delta}Sn_\delta Se$ indicate the opposite trend—that the system goes back from a topological to a trivial phase at higher temperature [4, 10, 11].

* antonius@lbl.gov

In this Letter, we compute from first-principles the topological phase diagram of $BiTl(S_{1-\delta}Se_\delta)_2$. The electron–phonon coupling and the temperature dependence of the electronic band energies is obtained from density functional perturbation theory (DFPT) [21–24], and we simulate doping with a linear mixing scheme. We show that the electron–phonon interaction causes a topological transition in the studied material, and indeed promotes the topological phase in $BiTlS_2$. However, this feature depends on the doping content. The opposite trend is predicted in $BiTlSe_2$, that is, the topological phase is suppressed at high temperature. We explain both behaviours by the symmetry of the phonon coupling potential, which was not considered in previous studies based on model hamiltonians.

Theory and methodology As a result of the electron–phonon coupling, the electronic energies acquire a temperature dependence given by

$$\varepsilon_{\mathbf{k}n}(T) = \varepsilon^0_{\mathbf{k}n} + \sum_\nu \int \frac{d\mathbf{q}}{\Omega_{BZ}} \Sigma^{ep}_{\mathbf{k}n}(\mathbf{q},\nu)\left[\, n_{\mathbf{q}\nu}(T) + \tfrac{1}{2}\,\right], \quad (1)$$

where $\mathbf{k}$ and n label the wavevector and band index of an electronic state, $\mathbf{q}$ and ν label the wavevector and branch index of a phonon mode, and Ω_{BZ} is the volume of the Brillouin zone. In this expression, the electron–phonon coupling self energy has been decomposed into the individual phonon modes' contributions. As we made use of the adiabatic approximation, all the temperature dependence of the electronic energies comes from the Bose-Einstein distribution of the occupations of the phonon modes $n_{\mathbf{q}\nu}(T)$, and the $\frac{1}{2}$ factor in Eq.(1) accounts for the zero-point renormalization. In the static theory of Allen, Heine and Cardona [25–27], the contribution of a phonon mode to the self energy is

$$\Sigma^{ep}_{\mathbf{k}n}(\mathbf{q},\nu) = \sum_{n'} \frac{|g_{\mathbf{k}nn'}(\mathbf{q},\nu)|^2}{\varepsilon_{\mathbf{k}n} - \varepsilon_{\mathbf{k}+\mathbf{q}n'} + i\eta} - \frac{|g^{DW}_{\mathbf{k}nn'}(\mathbf{q},\nu)|^2}{\varepsilon_{\mathbf{k}n} - \varepsilon_{\mathbf{k}n'} + i\eta}, \quad (2)$$

where $g_{\mathbf{k}nn'}(\mathbf{q},\nu)$ are the electron–phonon coupling matrix elements and η is a small positive real number. The first and second terms of Eq.(2) are called the Fan and Debye-Waller term respectively.

In most semiconductors and insulators, the self energy is positive for the last occupied band (i.e. reducing the hole energy) and negative for the first unoccupied band (i.e. reducing the quasi-electron energy). The band gap therefore closes with increasing temperature. The rationale behind this behavior is that, for a large band gap semiconductor, the top of the valence band would be repelled by the nearby occupied states with lower energies, while the bottom of the conduction band would be repelled by the nearby unoccupied states with higher energies. In the case of a topological insulator, the small band gap allows for a phonon-mediated interaction between the occupied and the unoccupied bands (since they are close in energy), and one has to give more consideration to anticipate the sign of the self-energy corrections.

Depending on the sign of the electron–phonon coupling induced self energy in Eq.(2), two possible scenario can occur with profound implications on the stability of the topological phase. In one case, the self energy would cause the band gap of a trivial insulator to close with increasing temperature, until a band inversion occurs, and the system reaches a topological phase at some critical temperature. At higher temperature, the inverted gap would further increase, thus stabilizing the topological phase. In the converse scenario, a system that is a topological insulator at low temperature could have its band gap shrink at higher temperature until the bands are reinverted and the system reaches a trivial phase. We show here that which one of these scenario occurs depends on the details of the system under consideration; it could even be reversed as the doping changes.

The method to compute phonon-related properties using DFPT is well established [28]. Besides providing the thermodynamical properties of solids, it has been successfully applied to the temperature dependence of electronic band structures [29–34]. In this work, we employ a linearized scheme to interpolate the phonon-related quantities at intermediate doping between two reference crystals structures.

The crux of the DFPT method for the electron-phonon coupling is the self-consistent calculation of the potential created by moving the atoms of the crystal in a periodic but non-commensurate unit amplitude displacement with wavevector $\mathbf{q}$:

$$V_{\kappa j}(\mathbf{q},\mathbf{r}) = \sum_{l} e^{i\mathbf{q}\cdot\mathbf{R}_l} \frac{\partial V^{\mathrm{SCF}}(\mathbf{r})}{\partial \tau_{l\kappa j}}, \tag{3}$$

where l labels a unit cell with lattice vector $\mathbf{R}_l$, κ labels an atom within the unit cell, j labels a Cartesian direction, and $\boldsymbol{\tau}$ is the position of an atom. From this periodic perturbation potential and the corresponding perturbed density, one evaluates the dynamical matrix, defined as the second-order derivative of the total energy with respect to unit displacements of two atoms. Its Fourier transform at wavevector $\mathbf{q}$ is given by

$$\Phi^{jj'}_{\kappa\kappa'}(\mathbf{q}) = \sum_{l} e^{i\mathbf{q}\cdot\mathbf{R}_l} \frac{\partial^2 E}{\partial \tau_{l\kappa j} \partial \tau_{0\kappa' j'}}. \tag{4}$$

The equation for the phonon modes with energies $\omega_{\mathbf{q}\nu}$ and polarization vectors $\xi^{\nu}_{\kappa j}$ is then

$$M_\kappa\ \omega^2_{\mathbf{q}\nu}\ \xi^{\nu}_{\kappa j}(\mathbf{q}) = \sum_{\kappa' j'} \Phi^{jj'}_{\kappa\kappa'}(\mathbf{q})\ \xi^{\nu}_{\kappa' j'}(\mathbf{q}), \tag{5}$$

where M_κ is the atomic mass.

Once the phonon modes and the perturbation potential are known, the electron–phonon self energy can be constructed. Defining an electron–phonon squared coupling matrix as

$$\Omega^{\kappa j,\kappa' j'}_{\mathbf{k}nn'}(\mathbf{q}) = \langle \mathbf{k}n|\, V^*_{\kappa j}(\mathbf{q},\mathbf{r})\, |\mathbf{k}+\mathbf{q}n'\rangle\, \langle \mathbf{k}+\mathbf{q}n'|\, V_{\kappa' j'}(\mathbf{q},\mathbf{r})\, |\mathbf{k}n\rangle\,, \tag{6}$$

we may write the squared electron–phonon coupling matrix elements as

$$|g_{\mathbf{k}nn'}(\mathbf{q},\nu)|^2 = \frac{1}{\omega_{\mathbf{q}\nu}} \sum_{\kappa,\kappa'} \sum_{j,j'} \Omega^{\kappa j,\kappa' j'}_{\mathbf{k}nn'}(\mathbf{q}) \big[\xi^{\nu}_{\kappa j}(\mathbf{q})\ \xi^{\nu *}_{\kappa' j'}(\mathbf{q})\big] \tag{7}$$

and their Debye-Waller counterpart as

$$|g^{DW}_{\mathbf{k}nn'}(\mathbf{q},\nu)|^2 = \frac{1}{2\omega_{\mathbf{q}\nu}} \sum_{\kappa,\kappa'} \sum_{j,j'} \Omega^{\kappa j,\kappa' j'}_{\mathbf{k}nn'}(0) \times \big[\xi^{\nu}_{\kappa j}(\mathbf{q})\ \xi^{\nu *}_{\kappa j'}(\mathbf{q}) + \xi^{\nu}_{\kappa' j}(\mathbf{q})\ \xi^{\nu *}_{\kappa' j'}(\mathbf{q})\big]. \tag{8}$$

We perform electronic structure and DFPT calculations on the reference systems $BiTlS_2$ and $BiTlSe_2$. To simulate a doping δ resulting in the stoechiometric formula $BiTl(S_{1-\delta}Se_\delta)_2$, we mix a quantity A computed in $BiTlS_2$ and $BiTlSe_2$ according to

$$A\big[\mathrm{BiTl}(\mathrm{S}_{1-\delta}\mathrm{Se}_\delta)_2\big] = (1-\delta) A\big[\mathrm{BiTlS}_2\big] + \delta A\big[\mathrm{BiTlSe}_2\big]. \tag{9}$$

The quantities A being mixed are the dynamical matrix Φ, the atomic masses M, the electron–phonon squared coupling matrix Ω and the eigenvalues ε. In doing so, we keep track of the parity eigenvalue of the electronic states at Γ. The electronic quantities (Ω, ε) are thus mixed between states with the same parity. This linear mixing scheme offers a simple procedure to treat intermediate doping. It ignores however the effect of disorder on the electronic structure and vibrational properties.

In this work, we retain only the electron–phonon coupling contribution to the self energy, and we neglect the

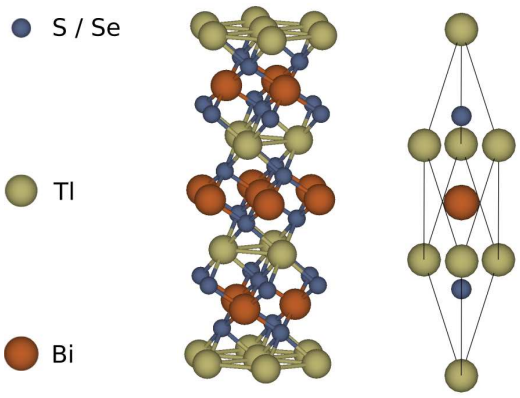

FIG. 1. Crystal structure of $BiTlS_2$ or $BiTlSe_2$ showing the conventional unit cell (left) and the primitive unit cell (right).

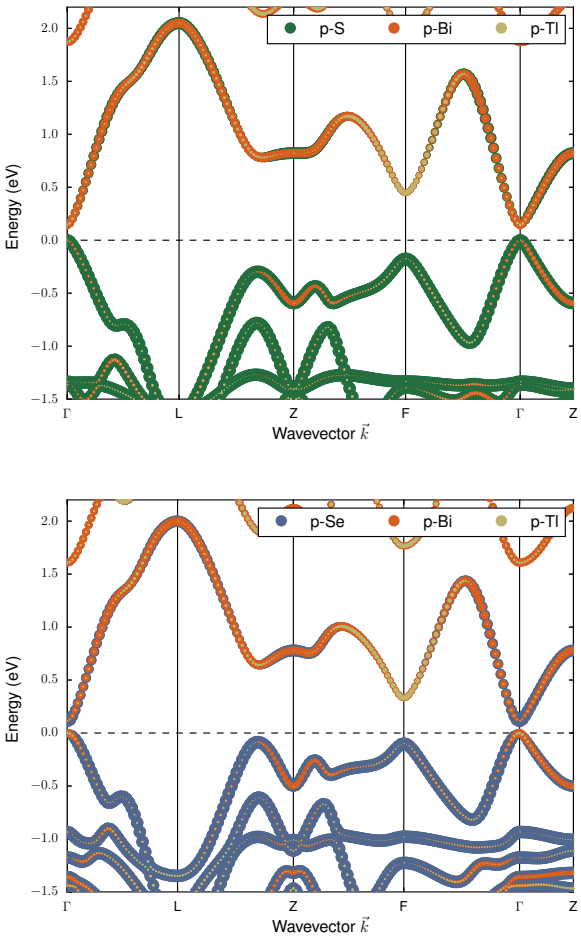

FIG. 2. Band structures of $BiTlS_2$ (top) and $BiTlSe_2$ (bottom). The size of the colored discs is propotional to the projection of the electronic wavefunctions onto various angular momenta around the atoms.

effect of thermal expansion of the lattice. While the change of the volume as a function of doping is taken into account, the temperature dependence of the eigenvalues at a given doping is computed for a fixed-volume experiment. Our DFT and DFPT calculations [35] were performed with Abinit [36] using ONCV pseudopotentials [37] and a revised PBE functional [38]. The choice of this exchange-correlation functional is motivated by the correct description of the material's band structure. A more accurate description of the electronic structure and the electron-phonon coupling strength would have to rely on *GW* calculations [31, 34, 39, 40]. However, the exchange-correlation functional chosen in this work yields the correct band gap and band topology for the materials under consideration, while allowing for the use of the DFPT method to obtain the lattice dynamics and the electron-phonon coupling. We therefore expect the electron-phonon coupling strength computed with this functional to be reasonably accurate.

Results and discussion The crystal structure of $BiTlS_2$ and $BiTlSe_2$ is a close-packed stacking of hexagonal planes whose unit cell contains a single formula unit [41], as shown in Fig.1. We obtained the lattice parameters by minimizing the internal stress, and relaxed the atomic coordinates until vanishing forces remained on the atoms. The resulting lattice parameters [42] are slightly overestimated compared to experiments [3].

The band structures of $BiTlS_2$ and $BiTlSe_2$ are quite similar in energy, but a distinct topology of the bands is revealed by the angular momentum decomposition of the electronic states, as shown in Fig.2. The p states around thallium are always associated with a negative parity, since this atoms is an inversion center of the crystal and is taken as the origin in our calculations. The p states around bismuth indicate a negative parity for the wavefunctions at Γ and F, and a positive parity at L and Z, since the application of inversion symmetry translates this atom into another primitive cell. In $BiTlS_2$, the characters of the last valence band and the first conduction band evolve smoothly through the Brillouin zone, resulting in a trivial phase with $Z_2 = 0$. In $BiTlSe_2$, the characters of these bands invert at Γ, resulting in a topological phase with $Z_2 = 1$.

Figure 3 shows the temperature dependence of the valence bands maximum (VBM) and the conduction bands minimum (CBM) for various intermediate doping between $BiTlS_2$ and $BiTlSe_2$. By tracking the critical temperature as a function of doping, we obtain the corresponding topological phase diagram, shown in Fig.4. In $BiTlS_2$ and for low doping ($\delta \lesssim 0.3$), the band gap closes as a function of temperature, promoting the topological phase above the critical temperature. At intermediate doping, the electron–phonon coupling self energy terms change sign but the system remains in the trivial state. The band gap now increases with temperature and no topological phase is found. Above the critical doping ($\delta \approx 0.55$) up to $BiTlSe_2$, the VBM and the CBM are

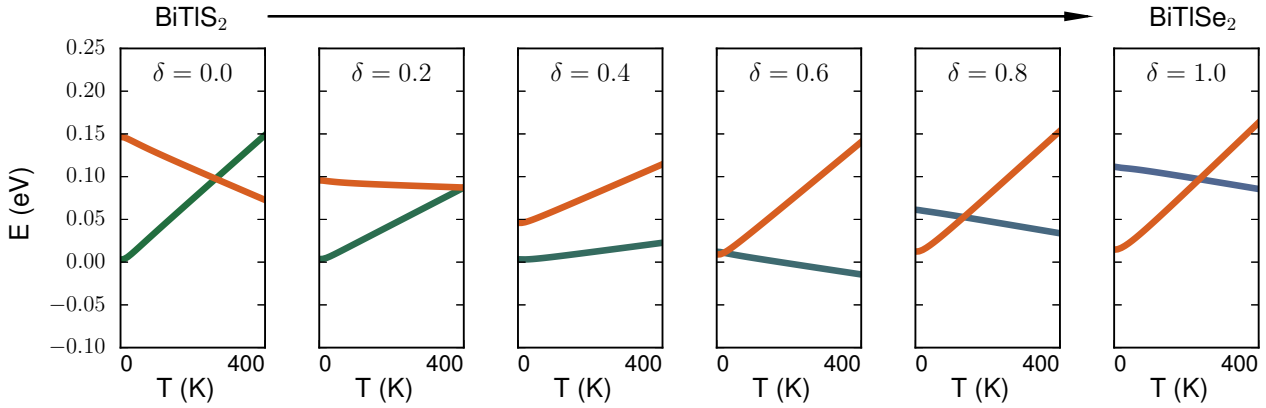

FIG. 3. Temperature dependence of the top of the valence bands and the bottom of the conduction bands for different doping between $BiTlS_2$ and $BiTlSe_2$.

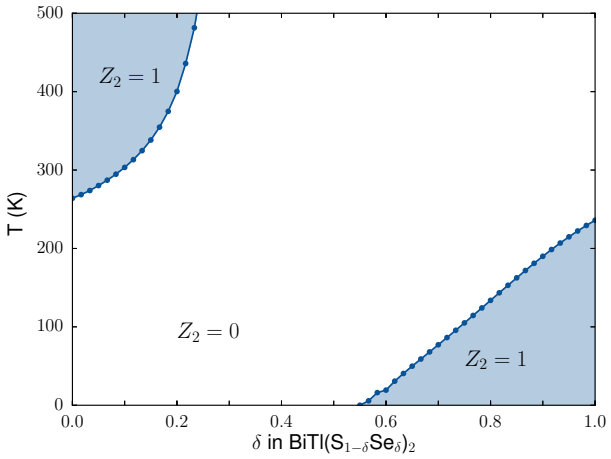

FIG. 4. Topological phase diagram of $BiTl(S_{1-\delta}Se_\delta)_2$ as a function of the doping parameter (δ) and temperature. The blue shaded region indicates the topological phase.

inverted, and again the inverted band gap closes with temperature. The system is driven back into the trivial phase above the critical temperature.

The sign flip of the self energy terms can be understood in terms of intra-band and inter-band scattering processes of the bands nearest to the band gap. These are the terms with the smallest energy denominators in the Fan self energy—the first term of Eq.(2)—making the dominant contributions to the eigenvalues renormalization. In the intra-band scattering, the VBM (CBM) couples to another state in the same band with lower (higher) energy, and this process closes the band gap. Conversely, in the inter-band scattering, the VBM (CBM) couples to a state in the first conduction band (last valence band), and this process opens the band gap. The strongest intra-band and inter-band interactions happen in the neighborhood of the Γ and F points in k-space, where the band gap reaches local minima.

The relative strenght of inter-band and intra-band interactions stems from the symmetry of the coupling potential. Rewrite the electron–phonon coupling elements as $g_{\mathbf{k}nn'}(\mathbf{q},\nu) = \langle \mathbf{k}+\mathbf{q}n'|\, V_{\mathbf{q}\nu}(\mathbf{r})\,|\mathbf{k}n\rangle$ with the phonon potential

$$V_{\mathbf{q}\nu}(\mathbf{r}) = \sum_{\kappa j} V_{\kappa j}(\mathbf{q},\mathbf{r})\xi^{\nu}_{\kappa j}(\mathbf{q}). \tag{10}$$

Due to inversion symmetry, the position $\boldsymbol{\tau}_\kappa$ of an atom κ is related to the position of its inversion partner $-\kappa$ in the same unit cell by $-\boldsymbol{\tau}_\kappa = \boldsymbol{\tau}_{-\kappa} + \mathbf{I}_\kappa$, where $\mathbf{I}_\kappa$ is a lattice vector. The consequence for the phonon polarization vectors is that inversion partners are related by

$$\xi^{\nu}_{-\kappa j}(\mathbf{q}) = -\lambda_{\mathbf{q}\nu} e^{i\mathbf{q}\cdot\mathbf{I}_\kappa}\xi^{\nu *}_{\kappa j}(\mathbf{q}), \tag{11}$$

with $\lambda_{\mathbf{q}\nu} = \pm 1$ defining the parity of the phonon vector. At time-reversal invariant momenta, the phonon potentials are parity eigenfunctions with

$$V_{\mathbf{q}\nu}(\mathbf{r}) = \lambda_{\mathbf{q}\nu} V_{\mathbf{q}\nu}(-\mathbf{r}). \tag{12}$$

Therefore, a phonon with odd parity ($\lambda_{\mathbf{q}\nu} = -1$) can only couple electronic states with opposite parities, and a phonon with even parity ($\lambda_{\mathbf{q}\nu} = +1$) can only couple electronic states with the same parity.

Since the parity of the bands is unchanged between Γ and F, we can make the following statement about the phonon modes at these points. In both $BiTlS_2$ and $BiTlSe_2$, the even phonon modes will promote the topological phase, and the odd phonon modes will promote the trivial phase. Furthermore, we note that at Γ and F, the even phonon modes are those where the pair of S or Se atoms move in opposite directions, while the Bi and Tl atoms do not move. As the sulfur atoms are being substituted for the heavier selenium atoms, the coupling with even phonon modes decreases, and the odd phonon

modes dominate. Therefore, the system transitions from a regime where the topological phase is promoted at high temperature to a regime where the trivial phase is promoted instead.

In summary, we observed, from first-principles calculations, a temperature-induced band inversion occuring in $BiTl(S_{1-\delta}Se_{\delta})_2$, and we computed the corresponding topological phase diagram in doping and temperature space. The non-trivial phase exists under two different regimes. In $BiTlS_2$ and for low doping, the topological phase is promoted above the critical temperature from a low-temperature trivial phase; in $BiTlSe_2$ and for high doping, the topological phase is observed only at low temperature and is suppresed above the critical temperature. Experimentally, non-trivial topological phases have been observed only at low temperatures so far. Our analysis indicates however that any topological insulator material containing light atoms forming inversion pairs could exhibit a topological phase that is promoted with temperature.

G. Antonius acknowledges fruitiful discussions with Ion Garate and Kush Saha. This research was supported by the National Science Foundation under grant DMR-1508412 which provided for basic theory and formalism, and by the Center for Computational Study of Excited-State Phenomena in Energy Materials funded by the U. S. Department of Energy, Office of Basic Energy Sciences, under Contract No. DE-AC02-05CH11231 at Lawrence Berkeley National Laboratory which provided for algorithm and code developments and simulations. The computational ressources were provided by the National Energy Research Scientific Computing Center (NERSC), a DOE Office of Science User Facility supported by the Office of Science of the U.S. Department of Energy under Contract No. DE- AC02-05CH11231, and the Extreme Science and Engineering Discovery Environment (XSEDE), which is supported by National Science Foundation Grant No. 787 ACI-1053575.

[1] M. Z. Hasan, S.-Y. Xu, and G. Bian, Physica Scripta **2015**, 014001 (2015).
[2] D. Hsieh, D. Qian, L. Wray, Y. Xia, Y. S. Hor, R. J. Cava, and M. Z. Hasan, Nature **452**, 970 (2008).
[3] S.-Y. Xu, Y. Xia, L. A. Wray, S. Jia, F. Meier, J. H. Dil, J. Osterwalder, B. Slomski, A. Bansil, H. Lin, R. J. Cava, and M. Z. Hasan, Science **332**, 560 (2011).
[4] P. Dziawa, B. J. Kowalski, K. Dybko, R. Buczko, A. Szczerbakow, M. Szot, E. Łusakowska, T. Balasubramanian, B. M. Wojek, M. H. Berntsen, O. Tjernberg, and T. Story, Nature Materials **11**, 1023 (2012).
[5] S.-Y. Xu, M. Neupane, C. Liu, D. Zhang, A. Richardella, L. Andrew Wray, N. Alidoust, M. Leandersson, T. Balasubramanian, J. Sánchez-Barriga, O. Rader, G. Landolt, B. Slomski, J. Hugo Dil, J. Osterwalder, T.-R. Chang, H.-T. Jeng, H. Lin, A. Bansil, N. Samarth, and M. Zahid Hasan, Nature Physics **8**, 616 (2012).
[6] X. Xi, C. Ma, Z. Liu, Z. Chen, W. Ku, H. Berger, C. Martin, D. B. Tanner, and G. L. Carr, Physical Review Letters **111**, 155701 (2013).
[7] M. Bahramy, B.-J. Yang, R. Arita, and N. Nagaosa, Nature Communications **3**, 679 (2012).
[8] S.-s. Li, W.-x. Ji, C.-w. Zhang, P. Li, and P.-j. Wang, Journal of Materials Chemistry C **4**, 2243 (2016).
[9] A. A. Reijnders, Y. Tian, L. J. Sandilands, G. Pohl, I. D. Kivlichan, S. Y. F. Zhao, S. Jia, M. E. Charles, R. J. Cava, N. Alidoust, S. Xu, M. Neupane, M. Z. Hasan, X. Wang, S. W. Cheong, and K. S. Burch, Physical Review B **89**, 075138 (2014).
[10] B. M. Wojek, P. Dziawa, B. J. Kowalski, A. Szczerbakow, A. M. Black-Schaffer, M. H. Berntsen, T. Balasubramanian, T. Story, and O. Tjernberg, Physical Review B **90**, 161202 (2014).
[11] B. M. Wojek, M. H. Berntsen, V. Jonsson, A. Szczerbakow, P. Dziawa, B. J. Kowalski, T. Story, and O. Tjernberg, Nature Communications **6**, 8463 (2015).
[12] Y. Zhang, C. Wang, L. Yu, G. Liu, A. Liang, J. Huang, S. Nie, Y. Zhang, B. Shen, J. Liu, H. Weng, L. Zhao, G. Chen, X. Jia, C. Hu, Y. Ding, S. He, L. Zhao, F. Zhang, S. Zhang, F. Yang, Z. Wang, Q. Peng, X. Dai, Z. Fang, Z. Xu, C. Chen, and X. J. Zhou, , arXiv:1602.03576 [cond-mat].
[13] H. Zhu, C. A. Richter, E. Zhao, J. E. Bonevich, W. A. Kimes, H.-J. Jang, H. Yuan, H. Li, A. Arab, O. Kirillov, J. E. Maslar, D. E. Ioannou, and Q. Li, Scientific Reports **3**, 1757 (2013).
[14] I. Garate, Physical Review Letters **110**, 046402 (2013).
[15] K. Saha and I. Garate, Physical Review B **89**, 205103 (2014).
[16] Z. Li and J. P. Carbotte, Physical Review B **88**, 195133 (2013).
[17] Li, Zhou and Carbotte, Jules P., Eur. Phys. J. B **88**, 87 (2015).
[18] T. Yoshida, R. Peters, and N. Kawakami, Physical Review B **93**, 045138 (2016).
[19] J. Kim and S.-H. Jhi, Physical Review B **92**, 125142 (2015).
[20] B. Monserrat and D. Vanderbilt also reported first-principle topological phase diagram calculations in the Bi_2Se_3 family compounds, as a function of pressure and temperature [43].
[21] S. Baroni, S. de Gironcoli, A. Dal Corso, and P. Giannozzi, Reviews of Modern Physics **73**, 515 (2001).
[22] S. Baroni, P. Giannozzi, and A. Testa, Physical Review Letters **58**, 1861 (1987).
[23] X. Gonze, Physical Review B **55**, 10337 (1997).
[24] X. Gonze and C. Lee, Physical Review B **55**, 10355 (1997).
[25] P. B. Allen and V. Heine, Journal of Physics C: Solid State Physics **9**, 2305 (1976).
[26] P. B. Allen and M. Cardona, Physical Review B **23**, 1495 (1981).
[27] P. B. Allen and M. Cardona, Physical Review B **27**, 4760 (1983).
[28] F. Giustino, , arXiv:1603.06965 [cond-mat].
[29] A. Marini, Physical Review Letters **101**, 106405 (2008).
[30] F. Giustino, S. G. Louie, and M. L. Cohen, Physical Review Letters **105**, 265501 (2010).
[31] G. Antonius, S. Poncé, P. Boulanger, M. Côté, and X. Gonze, Physical Review Letters **112**, 215501 (2014).

[32] S. Poncé, G. Antonius, Y. Gillet, P. Boulanger, J. Laflamme Janssen, A. Marini, M. Côté, and X. Gonze, Physical Review B **90**, 214304 (2014).

[33] G. Antonius, S. Poncé, E. Lantagne-Hurtubise, G. Auclair, X. Gonze, and M. Côté, Physical Review B **92**, 085137 (2015).

[34] B. Monserrat, Physical Review B **93**, 100301 (2016).

[35] The ground state calculation is performed with an 8×8×8 k-point grid and a kinetic energy cutoff of 50 Ha. The phonon wavevector sampling for the DFPT calculation is performed with an $8 \times 8 \times 8$ q-point grid for the full Brillouin zone, while the central region of the Brillouin zone is sampled with a $32 \times 32 \times 32$ q-point grid.

[36] X. Gonze, B. Amadon, P.-M. Anglade, J.-M. Beuken, F. Bottin, P. Boulanger, F. Bruneval, D. Caliste, R. Caracas, M. Côté, T. Deutsch, L. Genovese, P. Ghosez, M. Giantomassi, S. Goedecker, D. Hamann, P. Hermet, F. Jollet, G. Jomard, S. Leroux, M. Mancini, S. Mazevet, M. Oliveira, G. Onida, Y. Pouillon, T. Rangel, G.-M. Rignanese, D. Sangalli, R. Shaltaf, M. Torrent, M. Verstraete, G. Zerah, and J. Zwanziger, Computer Physics Communications **180**, 2582 (2009).

[37] D. R. Hamann, Physical Review B **88**, 085117 (2013).

[38] Y. Zhang and W. Yang, Physical Review Letters **80**, 890 (1998).

[39] I. Aguilera, C. Friedrich, and S. Blügel, Physical Review B **88**, 165136 (2013).

[40] I. Aguilera, C. Friedrich, G. Bihlmayer, and S. Blügel, Physical Review B **88**, 045206 (2013).

[41] S. V. Eremeev, G. Bihlmayer, M. Vergniory, Y. M. Koroteev, T. V. Menshchikova, J. Henk, A. Ernst, and E. V. Chulkov, Physical Review B **83**, 205129 (2011).

[42] The lattice parameters were optimized until the internal stress was below 10^{-8}Ha/Bohr^3, giving $a = 4.207\mathring{A}$ and $c = 22.492\mathring{A}$ for $BiTlS_2$, and $a = 4.372\mathring{A}$ and $c = 23.058\mathring{A}$ for $BiTlSe_2$, which are slightly overestimated compared to experiments ($a = 4.1\mathring{A}$, $c = 21.9\mathring{A}$ for $BiTlS_2$, and $a = 4.255\mathring{A}$, $c = 22.307\mathring{A}$ for $BiTlSe_2$) [3]. The only internal degree of freedom, u, is the relative height of the lowest sulfur or selenium atom. We relaxed the atomic coordinates until the forces on the atoms were below 10^{-7}Ha/Bohr, giving $u = 0.237$ for $BiTlS_2$, and $u = 0.239$ for $BiTlSe_2$.

[43] B. Monserrat and D. Vanderbilt, , arXiv:1608.00584 [cond-mat].